

Electrically Switchable Metadevices

Osman Balci^{1*}, Ertugrul Karademir², Semih Cakmakyapan³, Nurbek Kakenov¹,

Emre O. Polat⁴, Humeyra Caglayan⁵, Ekmel Özbay^{1,6}, Coskun Kocabas^{1,*}

¹*Department of Physics, Bilkent University, 06800 Ankara, Turkey*

²*School of Physics and CRANN, Trinity College Dublin, College Green, Dublin 2, Ireland*

³*Electrical Engineering Department, University of California Los Angeles, Los Angeles, California 90095, USA*

⁴*Electronics and Nanoscale Engineering, University of Glasgow, Glasgow, G12 8QQ, UK*

⁵*Department of Electrical and Electronics Engineering, Abdullah Gul University, 38039 Kayseri, Turkey*

⁶*Nanotechnology Research Center—NANOTAM, Bilkent University, 06800 Ankara, Turkey*

Corresponding authors' email: obalci@fen.bilkent.edu.tr, ckocabas@fen.bilkent.edu.tr

Metamaterials bring sub-wavelength resonating structures together to overcome the limitations of conventional matter. The realization of active metadevices has been an outstanding challenge that requires electrically reconfigurable components operating over a broad spectrum with a wide dynamic range. The existing capability of metamaterials, however, is not sufficient to realize this goal. Here, integrating passive metamaterials with active graphene devices, we demonstrated a new class of electrically controlled metadevices. These metadevices enable efficient control of both amplitude (> 50 dB) and phase ($> 90^\circ$) of electromagnetic waves. In this hybrid system, graphene operates a tunable Drude metal that controls the radiation of the passive metamaterials. Furthermore, by integrating individually addressable arrays of metadevices, we demonstrated a new class of spatially varying digital metasurfaces where the local dielectric constant can be reconfigured with a bias voltage. Our approach is general enough to implement various metamaterial systems that could yield new applications ranging from electrically switchable clocking devices to adaptive camouflage systems.

Metamaterials have been a powerful tool to control and manipulate electromagnetic waves and their interaction with matter¹⁻³. The integration of passive metamaterials with a variety of tuning mechanisms has been examined to generate active metadevices that have novel functionalities⁴⁻⁷. Based on the tuning mechanisms, these active metadevices can be classified into three general categories, which are circuit-, material-, and physical-based metadevices⁸. The circuit-based metadevices use variable capacitors or switches to alter the lumped elements of the equivalent circuit. For instance, the reverse bias voltage applied on a varactor integrated on a split ring resonator changes the effective capacitance of the equivalent circuit⁹⁻¹². Material-based metadevices rely on controlling bulk material properties, such as the permittivity, permeability, or conductivity of the individual unit cell under an external stimulus^{7,13-18}. The conductivity of semiconducting material deposited in the split gap can be tuned by illumination and thereby alters the resonance frequency of the metamaterial. Similarly, interconnected metamaterials fabricated on a semiconductor surface were used to tune the depletion area that alters the free carrier absorption^{19,20}. On the other hand, physical-metadevices tune their response by changing their shape or relative position of sub-components (such as split gap)²¹⁻²⁵. For example, micro electro mechanical (MEMs) based devices can tune the resonance frequency of metadevices in terahertz spectra²³. Although these devices provide some degree of tunability, their performances are limited to narrow spectra with a small dynamic range due to the material and fabrication limitations. These technologies would greatly benefit from a material that yields large tunability over broad spectra. None of the existing materials provide these challenging requirements. Furthermore, the requirement for electrically controlled tunability places another challenge for practical applications of metadevices.

2-dimensional crystals provide new perspectives for reconfigurable smart surfaces that can be used for the realization of electrically tunable metadevices²⁶⁻³⁰. The thickness of 2D crystals is much shorter than the effective wavelength and, therefore, their electromagnetic response solely originates from the charge carriers. Recent studies have shown that tuning the density of high mobility free carriers on graphene yield an unprecedented ability to control light-matter interaction over a very broad spectra ranging from visible to microwave frequencies^{31,32}. By engineering the shape or doping level, the plasmon frequency of graphene can be tuned in IR and THz frequencies^{28,33}. In another approach, graphene is coated on a metamaterial^{34,35} or optical antennas^{36,37} to yield electrically tunable metadevices. Tuning the charge density alters the effective dielectric constant of the medium. However, these devices are not suitable for practical

applications due to limited tunability³⁸. Recently, we discovered a simple device structure consisting of an electrolyte medium sandwiched between two large area graphene electrodes. This geometry permits an efficient mutual gating between two graphene electrodes that yields charge densities on the order of 10^{14} cm^{-2} ³⁹. Using this supercapacitor structure, we fabricated various optoelectronic devices including optical modulators^{39,40}, electrochromic devices⁴¹, and switchable radar absorbing surfaces⁴². In this paper, using graphene supercapacitors incorporated with metallic split ring resonators, we demonstrated a new type of electrically controlled metadevices. These metadevices are based on tunable high mobility free carriers on graphene to introduce electrically tunable dissipation in the resonator capacitively coupled to the graphene electrodes.

Integrating split ring resonators (SRR) in close proximity of the graphene surface yields a new type of hybrid metamaterial whose resonance can be tuned by various means. Previous attempts to integrate graphene with metamaterials yielded very limited modulation in infrared and terahertz frequencies^{33,35}. Here, we use a different approach using microwave metamaterials capacitively coupled to large area graphene that yields substantial tunability. Figure 1a shows a schematic drawing of this hybrid structure. The presence of graphene in close proximity of the SRR introduces additional electrical losses due to the sheet resistance of graphene. The equivalent small signal model of the hybrid structure is shown Figure 1b. The ring and split gap provide the inductance, L , and the capacitance, C , respectively. The resistor, R , models the dissipation on the metal due to the electrical and radiation resistance. In our design, the SRR is capacitively coupled to graphene ($C_c = \frac{\epsilon \epsilon_0}{d}$, the coupling capacitance, ϵ is the dielectric constant of the medium and ϵ_0

is the free space permittivity). The graphene layer can be modeled by the sheet resistance ($R_G = \frac{1}{\sigma(n)}$, where $\sigma(n)$ is a charge dependent sheet conductance of graphene) and quantum

capacitance of the graphene electrodes ($C_Q = \frac{2e^2}{\hbar v_F} \sqrt{\frac{n}{\pi}}$ where e is the elementary charge, v_F is the

Fermi velocity, n is the charge density). The quantum capacitance of unintentionally doped graphene layer ($C_Q \sim 0.5 \text{ } \mu\text{F}/\text{cm}^2$) is much larger than the serial coupling capacitance ($C_c \sim 5 \text{ pF}/\text{cm}^2$) and, therefore, in the small circuit model we can neglect its contribution⁴³.

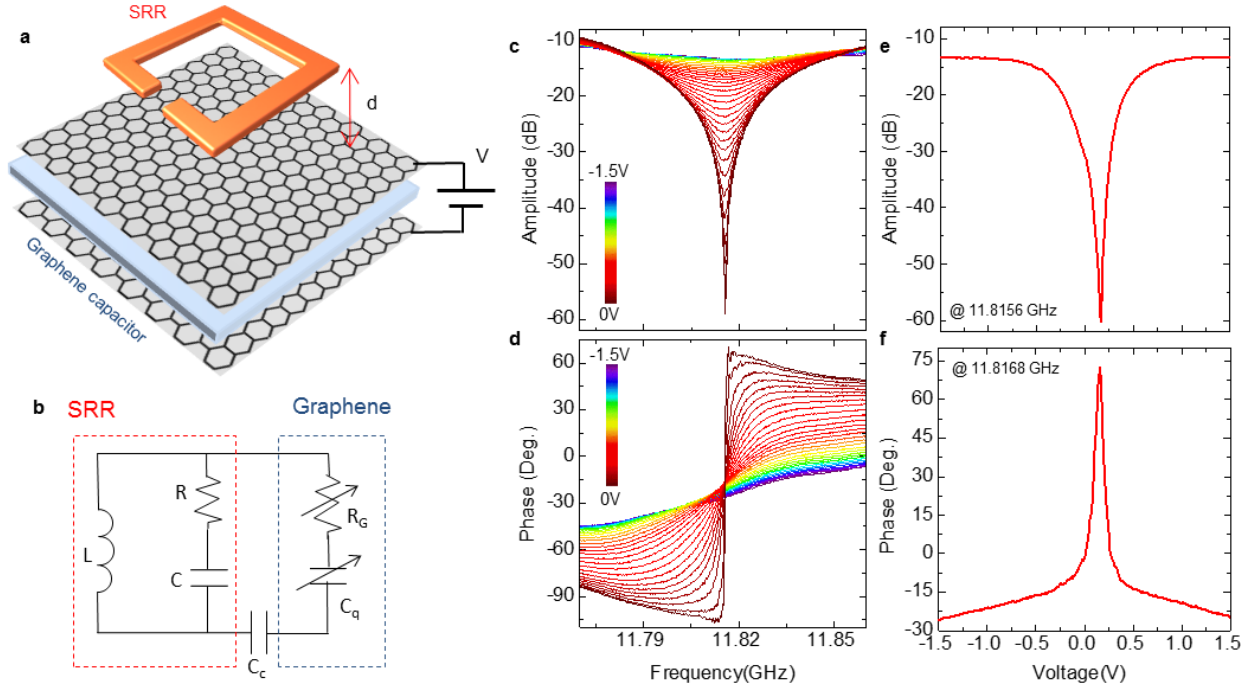


Figure 1. Electrically tunable metamaterials: **a**, Schematic representation of the hybrid metamaterial system consisting of split-ring resonator capacitively coupled to the graphene electrodes. The capacitive coupling is defined by the SRR-graphene separation, d . **b**, Small-signal equivalent circuit model of the metadvice. SRR is represented by the L , R , C lump circuit elements; the graphene layer is modeled by the variable sheet resistance, R_G and quantum capacitance, C_Q . C_c models the capacitive coupling. **c,d**, Spectrum of the magnitude and phase of the transmittance (S_{21}) at various bias voltages. The color bar shows the bias voltage. **e,f**, The variation of the amplitude and phase of the transmittance with the bias voltage.

We can tune the electrical resonance of the metamaterials by changing the charge density on graphene layer via ionic gating. The technical challenge for graphene based microwave devices is the requirement of large area devices due to the centimeter scale wavelength (i.e. $\lambda = 3$ cm at 10 GHz). The ability to synthesize large area graphene with chemical vapor deposition on copper foils enables us to realize the proposed microwave metamaterials⁴⁴. Graphene electrodes were synthesized on copper foils using a chemical vapor deposition system and then we transferred them onto flexible PVC substrates using the hot lamination technique. Then, we etch laminated copper foils in a 5 mM FeCl_3 aqueous solution. We first put a paper tissue with a thickness of 40 μm

between two graphene electrodes as a spacer and then we soaked ionic liquid (1-Butyl-3-methylimidazolium hexafluorophosphate) into the tissue (Supplementary Note 1 and Figure 1-5). This device structure resembles supercapacitors formed by single layer graphene electrodes. The electrolyte permits mutual electrolyte gating between the graphene electrodes without using any metallic gate electrodes. Under an external bias voltage, the electrolyte gets polarized and gates the graphene electrodes. The graphene electrode connected to the negative voltage gets electron-doped (n-doped), whereas the other one gets hole-doped (p-doped). At zero volts, the sheet resistance of undoped graphene is around 2.5 k Ω and decrease down to 0.7 k Ω at ± 3 V. The charge density on the graphene electrodes changes between 3×10^{11} to 0.5×10^{14} cm $^{-2}$ (Supplementary Figure 5). The metallic SRR were fabricated on another PVC film by printing the SRR shapes on previously laminated 10 μ m thick copper foil followed by the chemical etching of copper (Supplementary Note 2 and Figure 6). The electromagnetic simulations (Supplementary Note 3 and Figure 7) led us to find the optimum graphene-SRR separation of 2.4 mm that provides the highest modulation amplitude. After assembling the device, we measured the scattering parameters using a broadband horn antenna as a source and a dipole antenna as a receiver connected to a two-port network analyzer. To excite the electrical resonance, we polarized the electric field along the split gap of SRR. This active device yields an unprecedented ability to control the intensity and phase of the transmitted electromagnetic waves. Figure 1c and 1d show the amplitude and phase of the transmittance (S_{21}) measured through the fabricated device at various bias voltages. At 0 V, the device yields a resonance at 11.8156 GHz with a resonance transmittance of -60 dB. When we applied a bias voltage, electrons and holes accumulated on the graphene electrodes and yielded significant damping that diminishes the resonant behavior. At 1.5 V, for example, the resonance transmittance is -12 dB. Figure 1e and 1f show the voltage dependence of the amplitude of transmittance at resonance (11.8156 GHz) and the phase (at 11.8168 GHz). The phase of the transmitted signal varies from -30° to 70° . We observed a symmetric behavior when we changed the polarity of the bias voltage owing to the ambipolar behavior of the graphene electrodes. The charge neutrality point is slightly shifted to the positive voltages. Our approach is independent of the structure of the metamaterials. We tested various metamaterial systems and observed similar electrical tunability. (Supplementary Note 4 and Figure 9-14)

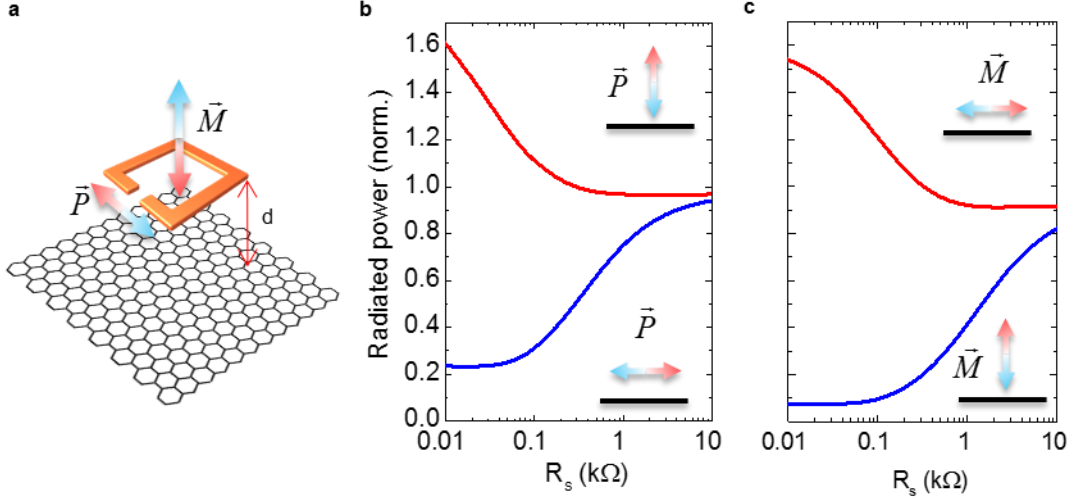


Figure 2. Electric and magnetic dipole emitters near a tunable 2D-Drude metal. **a**, Schematic representation of induced electric and magnetic dipoles on an SRR independent from the direction of polarization of incident radiation. **b,c**, Normalized radiated power of electrical and magnetic dipoles at different orientations plotted against the sheet resistance of the Drude metal. The dipoles are placed at a distance of 2 nm from the interface. The inset shows the orientation of the dipole emitters with respect to the sheet resistance of tunable interface shown by the black lines.

To understand the electrical tunability of the hybrid system, we developed a quantitative model using electric and magnetic dipole emitters. The scattering of electromagnetic waves by a SRR can be described by the coherent superposition of the incident and the radiated electromagnetic waves emitted by the induced multipoles on the metallic structures. When the wavelength of radiation is large compared to the size of the SRR, the lowest order of induced multipoles are enough to quantify the scattering⁴⁵. Figure 2a shows the induced electrical and magnetic dipoles on SRR. These induced dipoles define the electrical and magnetic response of the metadevices, respectively. To understand the physics behind the tunable metadevices, we studied the radiation of dipole emitters near a tunable Drude metal that can model the effect of the graphene electrodes. Although the quenching of molecular emitters near metals and graphene surface has been studied before^{46,47}, the radiation of long wavelength electrical and magnetic dipole emitters near tunable metals remained unexplored due to the lack of an electrically tunable material. Electrical control of the charge density on large area graphene provides a unique opportunity to study this behavior. In our model, we studied the total radiated power from a long-

wavelength dipole emitter (at 10 GHz) placed near a conducting interface ($d = 2$ mm) with a tunable sheet resistance of R_s . Figure 2b and 2c show the variation of the radiated power from an electrical and magnetic dipole as the sheet resistance of the interface changes from 10Ω to $10 \text{ k}\Omega$. Depending on the orientation of the dipole (inset in Figure 2b and 2c), we observed both the quenching and enhancement of the radiated power. When the electrical dipole is in the plane of the conducting interface, we observe a significant quenching as the conductivity of the interface increases. However, when the dipole is perpendicular to the interface, the radiated power is enhanced. This behavior can also be understood with induced image dipoles due to the conducting interface. The strength of the induced dipole varies with the conductivity. The simulated results show similar but more pronounced effects for a magnetic dipole with opposite orientations. These results confirm that both electric and magnetic resonance of a metamaterial can be controlled by the electrical gating of graphene. The ability to control the effective strength of dipole emitters by tuning the charge density on the graphene layer opens new active functional metamaterials. The model based on multipoles near Drude metal also provides a handy tool to design the metadevices (Supplementary Note 5 and Figures 15-20).

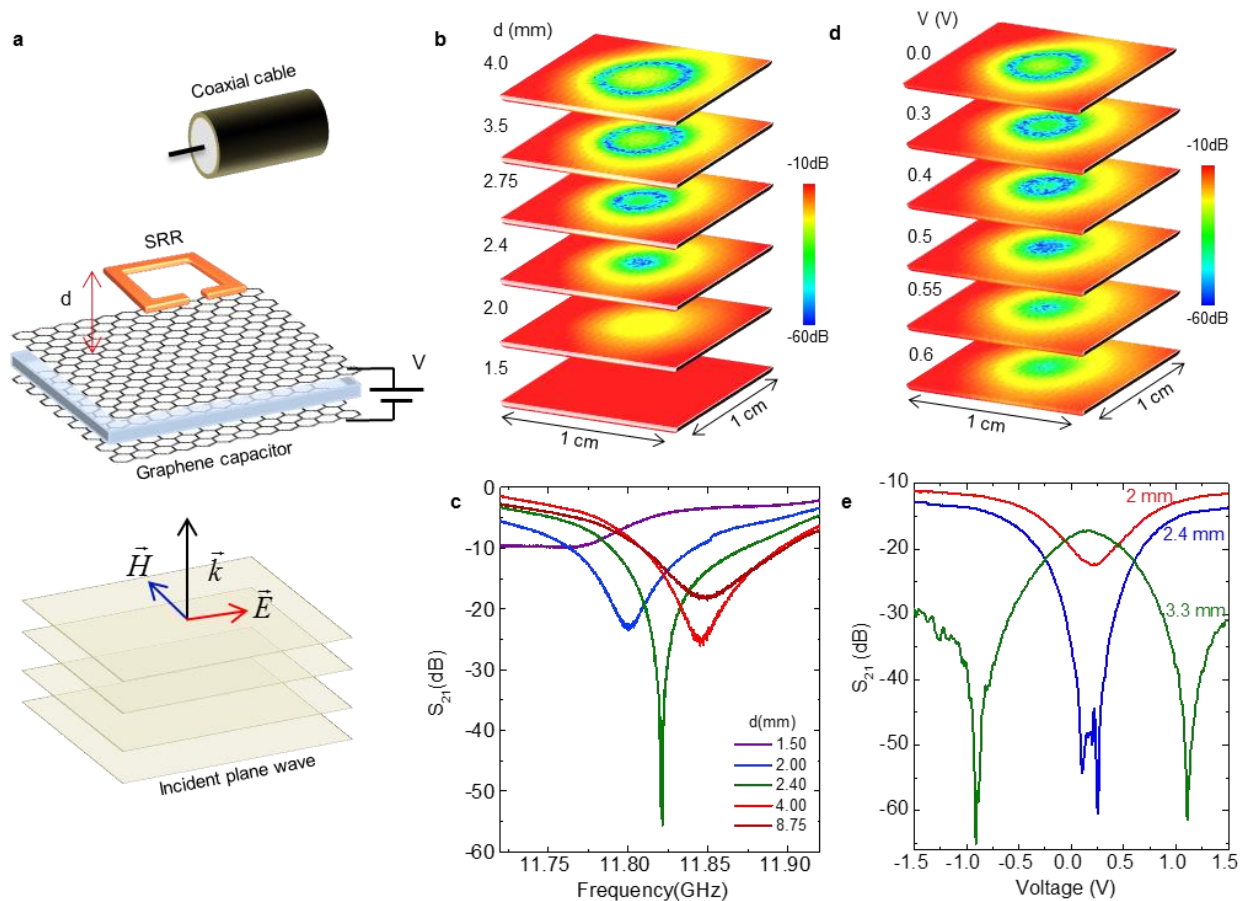


Figure 3. Near-field characterization of the active metadevices: **a**, Near-field scanning technique to map the local scattering parameter (S_{21}) of the device. Scattering parameter provides the magnitude of the local electric field along the direction of the antenna. **b,c** Spatial map and the spectrum of the local scattering parameter of the metadevices probed by a dipole antenna at different graphene-SRR distance. **d,e** Voltage dependence of the spatial map and magnitude at the center of the local scattering parameters of the device.

To explore the tunability of electric field distribution of active metadevices, we used a near-field scanning technique to map the local electric field distributions⁴⁸. We placed the device on a computer controlled motorized stage and recorded the spectrum of the local scattering parameter using a monopole antenna connected to a network analyzer (Figure 3a and Supplementary Figure 12). First, we examined the critical coupling condition between the graphene electrode and SRR at zero bias voltage. Figure 3b shows the measured local electric field distribution of metadevices at different graphene-SRR separation. We observed that in the near-field of the metadevices, the complete extinction of the microwave signal (i.e. resonance) occurs on a ring-shape region whose radius depends on the graphene-SRR separation. When the graphene is very close (< 2 mm) to the SRR, the resonance diminishes due to the large dissipation on graphene. This behavior is a microwave analog of the quenching of a dipole emitter placed on a metallic surface. Figure 3c shows the transmittance spectrum at the center. By tuning the separation, we can obtain the critical coupling condition such that the resonance condition occurs along the forward direction. At this critical distance, we obtained the largest modulation of 50 dB. Then, we measured the variation of the near-field distribution as a function of bias voltage (Figure 3c). With the increasing charge density on graphene electrodes, the extinction ring shrinks further and diminishes at large voltages. The observed behavior is quantified in Figure 3c that shows the voltage dependence of the scattering parameter for three different graphene-SRR distances. Because of the ambipolar nature of graphene electrodes, we observed two resonances at positive and negative voltages. The slight asymmetry is due to the difference of Dirac point of the graphene electrodes (Supplementary Note 6 and Figures 21-23).

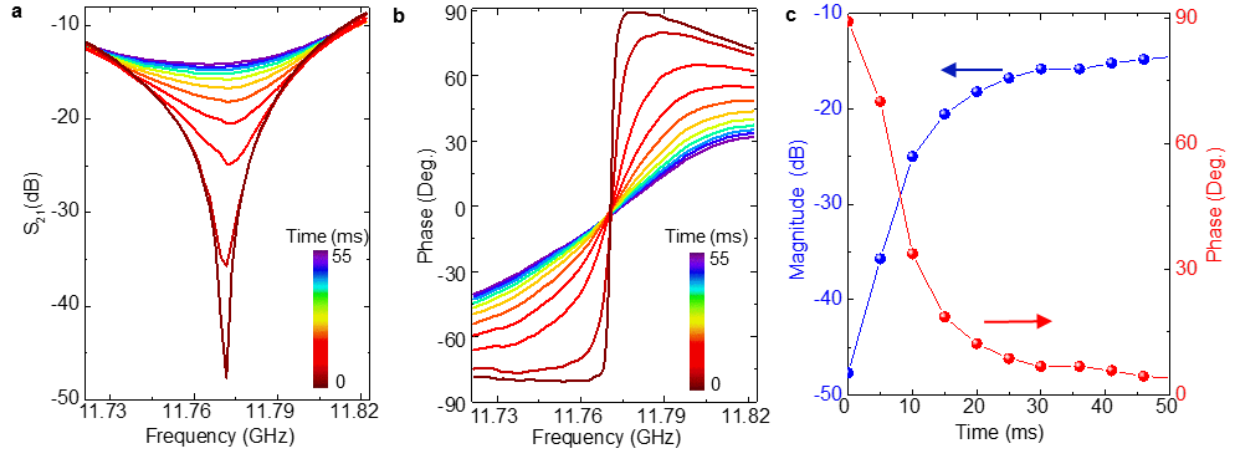


Figure 4: Time-response of the metadevices: a,b, Time-resolved spectrum of the amplitude and phase of the transmittance (S_{21}) of the metadevices after we applied a bias voltage of 1.5 V. **c**, and the variation of the resonance transmittance and phase of the device.

After studying the tunability of the metadevices, we examined their switching behavior. We measured the time-resolved microwave spectrum of the scattering parameters of the device after we applied a step-like bias voltage of 1.5 V. Figure 4a and 4b shows the evolution of the amplitude and the phase of S_{21} . As the capacitor charges, the resonance transmittance increases from -50 to -15 dB in 20 ms. Similarly, the phase changes from 90 degree down to 0 near the resonance frequency. The time response of the device is limited with the charging time of the graphene capacitor that scales inversely with the area of the device. The device characterized in Figure 4 has dimensions of $15 \times 15 \text{ cm}^2$ that results in an RC time constant of approx. 20 ms.

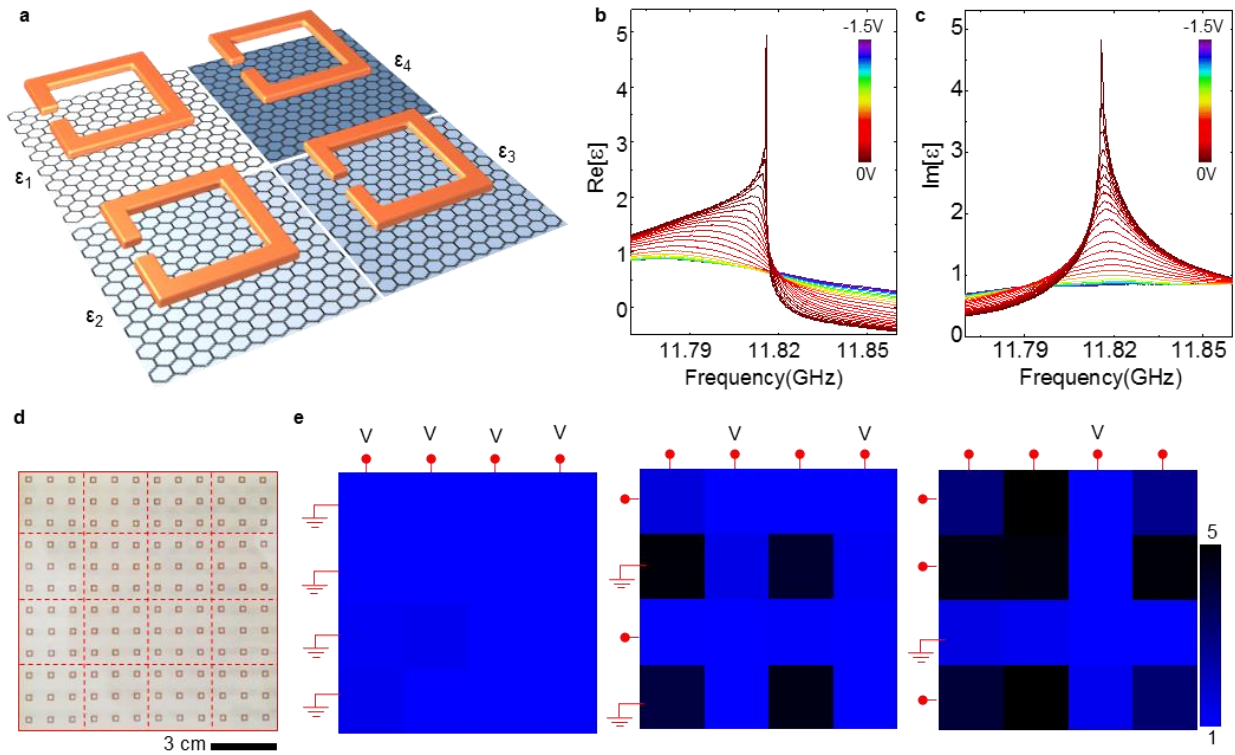


Figure 5. Electrically-reconfigurable spatially-varying digital metamaterials: **a** Schematic drawing of a digital metamaterial with individually addressable pixels. Controlling the charge density on individual pixels allows us to reconfigure the local dielectric constant. **b,c** The spectrum of the calculated real and imaginary part of the effective dielectric constant of a single pixel under different bias voltages. **d**, The spatial map of the real part of the effective dielectric constant of the device at the resonance for different voltage configurations. The effective dielectric constant of the pixels is controlled by passive matrix addressing.

To show the promises of the approach, we would like to demonstrate the spatial tuning of metamaterials that could open new applications in transformation optics⁴⁹. Transformation optics is an emerging field of research aiming to conceal an object by bending or distorting electromagnetic waves using spatially varying metamaterials^{50,51}. Ability to control the spatial variation of permittivity and permeability by electrical means would yield new vistas for the adaptive electromagnetic cloaking and camouflage. By integrating arrays of individually addressable metadevices, our approach can be used for voltage controlled adaptive transformation optics. Figure 5 shows the schematic of the multipixel device. By controlling the local charge

density on a pixelated surface by passive matrix addressing, we demonstrate an electrically-reconfigurable spatial-varying metadevices. We fabricated a large area metadevices with 4x4 arrays of active pixels. Each pixel contains 9 SRRs (3x3). We measured the scattering parameter at the center of the pixels and then calculated the local dielectric function. Figure 5b and 5c show the calculated real and imaginary part of the effective dielectric constant. By accumulating charges on a pixel, the local dielectric constant varies from 5 down to 0.8. Figure 5d shows spatial maps of the real part of the dielectric constant of the pixelated device at different voltage configurations. We were able to reconfigure the spatial variation of the dielectric constant over the device by changing the voltage applied to the rows and columns. The cross coupling between the pixels is due to the passive matrix addressing. These devices are on thin flexible substrates that can be wrapped around nonplanar objects for cloaking purposes (Supplementary Note 7 and Figures 24-28).

The results presented here confirm a promising approach for electrically controlled metadevices. The core idea of the approach is based on the electrical tuning of effective strength of a dipole emitter placed close to a tunable Drude metal. Electrostatic tuning of the charge density on graphene yields broadband controllability on the response of metamaterials both in near-field and far-field (Supplementary Note 8 and Figures 29-32). These metadevices enable the efficient control of both amplitude (> 50 dB) and phase ($> 90^\circ$) of electromagnetic waves. To show the promising uses of the approach, we demonstrated electrically reconfigurable spatially varying metamaterials. The operation frequency of these metadevices can be easily scaled down to the terahertz frequencies. Large modulation depth, simple device architecture and mechanical flexibility are the key attributes of the graphene-enabled metadevices. We anticipate that the presented approach could lead to new applications ranging from electrically switchable cloaking devices to adaptive camouflage systems in microwave and terahertz frequencies.

Methods summary:

Synthesis of large area graphene: We synthesized large area graphene using a chemical vapor deposition system on ultra-smooth copper foils with 0.1 mm surface roughness (Mitsui mining and smelting company, LTD, B1-SBS). We cut copper foil by 7 cm x 14 cm and put on a flat quartz holder with a width of 6 cm and length of 30 cm. We placed the holder into a quartz chamber with a diameter of 8 cm, and we heated the chamber under 100 sccm H₂ flow. When the temperature reached 1035°C, we started to grow graphene by sending 10 sccm CH₄ for 1 min. During the growth, we used CH₄ and H₂ gases with a partial pressure of 1.5 Torr and 3 Torr, respectively. We cooled the chamber under 100 sccm H₂ flow after terminating the graphene growth (Supplementary Figure 1).

Transfer of large area graphene with hot lamination: After growing large area single layer graphene on ultra-smooth copper foils, we transferred graphene on a large area flexible PVC substrate. We used a hot laminating machine and a standard PVC film for hot lamination. One side of the PVC film is smooth and the other side is rough, which melts at nearly 100°C. We aligned two graphene grown copper foils as the graphene is on their top and two long edges are nearly touching each other on a standard A4 sheet of paper. Then, we laid the PVC film on copper foils and paper as the rough side is facing the copper foils and paper. We laminated the paper-copper foils-PVC stack in a hot laminating machine at nearly 100°C (Supplementary Figure 1).

Fabrication of a large area graphene supercapacitor: We used two layers of graphene transferred on a laminating film substrate to fabricate a large area graphene supercapacitor. A paper tissue with a thickness of 40 μm was used as a spacer between two graphene electrodes. We first put the tissue on top of one graphene electrode and then we put ionic liquid (1-Butyl-3methlimidazolium hexafluorophosphate). We placed the top graphene electrode, and let the ionic liquid disperse between the two graphene electrodes (Supplementary Fig. 4).

Fabrication of metamaterials: To fabricate metamaterial structures, we laminated 75 μm thick PVC laminating film on 10 μm thick copper foils. We printed the metamaterial structure on the copper foils using HP color laser jet printer (CP2020). We etched the copper in a nitric acid solution. The printed toner function as an etch mask on copper. With this technique we can define metadevices as small as 80 μm (Supplementary Fig. 6).

Electrical characterization of the device: We used an HP-4284A LCR meter for the capacitance and resistance measurements. We used 100 mV AC voltage superimposed on a variable DC voltage between -3 to 3 V. A serial capacitance and resistance model was used to extract the capacitance and resistance of the device (Supplementary Note 1 and Figure 5).

Microwave measurements: We used a Keysight-E5063A network analyzer for the microwave characterization of our device. We connected a horn antenna to one channel and a 1.5 cm long monopole antenna to the other channel of the network analyzer to measure S-parameters in the 7-15GHz range. The active metadevice was placed at a specific distance above the monopole antenna and the horn antenna was used to propagate microwaves in the air. The device is placed on a computer controlled motorized stage with 1 μm spatial resolution. Both the amplitudes and phases of the received signals were recorded for each location. The monopole antenna was aligned along the electric field of the horn antenna. We connected the Keithley 2400 source measure unit to apply voltage bias. We tuned the voltage manually and recorded the scattering parameters (Supplementary Figure 8).

References:

- 1 Tao, H., Padilla, W. J., Zhang, X. & Averitt, R. D. Recent Progress in Electromagnetic Metamaterial Devices for Terahertz Applications. *IEEE J Sel Top Quant* **17**, 92-101, doi:Doi 10.1109/Jstqe.2010.2047847 (2011).

- 2 Pendry, J. B., Schurig, D. & Smith, D. R. Controlling electromagnetic fields. *Science* **312**, 1780-1782, doi:DOI 10.1126/science.1125907 (2006).
- 3 Ozbay, E. Plasmonics: Merging photonics and electronics at nanoscale dimensions. *Science* **311**, 189-193, doi:DOI 10.1126/science.1114849 (2006).
- 4 Shin, D. *et al.* Broadband electromagnetic cloaking with smart metamaterials. *Nature communications* **3**, doi:Artn 1213
Doi 10.1038/Ncomms2219 (2012).
- 5 Zheludev, N. I. & Kivshar, Y. S. From metamaterials to metadevices. *Nature Materials* **11**, 917-924, doi:Doi 10.1038/Nmat3431 (2012).
- 6 Urzhumov, Y. *et al.* Electronically reconfigurable metal-on-silicon metamaterial. *Physical Review B* **86**, doi:Artn 075112
Doi 10.1103/Physrevb.86.075112 (2012).
- 7 Goldflam, M. D. *et al.* Reconfigurable gradient index using VO₂ memory metamaterials. *Applied Physics Letters* **99**, doi:Artn 044103
Doi 10.1063/1.3615804 (2011).
- 8 Turpin, J. P., Bossard, J. A., Morgan, K. L., Werner, D. H. & Werner, P. L. Reconfigurable and Tunable Metamaterials: A Review of the Theory and Applications. *Int J Antenn Propag*, doi:Artn 4298737
Doi 10.1155/2014/429837 (2014).
- 9 Hand, T. H. & Cummer, S. A. Reconfigurable Reflectarray Using Addressable Metamaterials. *Ieee Antenn Wirel Pr* **9**, 70-74, doi:Doi 10.1109/Lawp.2010.2043211 (2010).
- 10 Costa, F., Monorchio, A. & Vastante, G. P. Tunable High-Impedance Surface With a Reduced Number of Varactors. *Ieee Antenn Wirel Pr* **10**, 11-13, doi:Doi 10.1109/Lawp.2011.2107723 (2011).
- 11 Reynet, O. & Acher, O. Voltage controlled metamaterial. *Applied Physics Letters* **84**, 1198-1200, doi:Doi 10.1063/1.1646731 (2004).
- 12 Aydin, K. & Ozbay, E. Capacitor-loaded split ring resonators as tunable metamaterial components. *J Appl Phys* **101**, doi:Artn 024911
Doi 10.1063/1.2427110 (2007).
- 13 Werner, D. H., Kwon, D. H. & Khoo, I. C. Liquid crystal clad near-infrared metamaterials with tunable negative-zero-positive refractive indices. *Optics Express* **15**, 3342-3347, doi:Doi 10.1364/Oe.15.003342 (2007).
- 14 Gardner, D. F., Evans, J. S. & Smalyukh, I. I. Towards Reconfigurable Optical Metamaterials: Colloidal Nanoparticle Self-Assembly and Self-Alignment in Liquid Crystals. *Mol Cryst Liq Cryst* **545**, 1227-1245, doi:Doi 10.1080/15421406.2011.571966 (2011).
- 15 Golovin, A. B. & Lavrentovich, O. D. Electrically reconfigurable optical metamaterial based on colloidal dispersion of metal nanorods in dielectric fluid. *Applied Physics Letters* **95**, doi:Artn 254104
Doi 10.1063/1.3278442 (2009).
- 16 Han, J. & Lakhtakia, A. Semiconductor split-ring resonators for thermally tunable terahertz metamaterials. *J Mod Optic* **56**, 554-557, doi:Doi 10.1080/09500340802621785 (2009).
- 17 Han, J. G., Lakhtakia, A. & Qiu, C. W. Terahertz metamaterials with semiconductor split-ring resonators for magnetostatic tunability. *Optics Express* **16**, 14390-14396, doi:Doi 10.1364/Oe.16.014390 (2008).

- 18 Wang, J. Q., Liu, S. C., Guruswamy, S. & Nahata, A. Reconfigurable liquid metal based terahertz metamaterials via selective erasure and refilling to the unit cell level. *Applied Physics Letters* **103**, doi:Artn 221116
Doi 10.1063/1.4837675 (2013).
- 19 Chen, H. T. *et al.* Active terahertz metamaterial devices. *Nature* **444**, 597-600, doi:Doi 10.1038/Nature05343 (2006).
- 20 Chen, H. T. *et al.* A metamaterial solid-state terahertz phase modulator. *Nature Photonics* **3**, 148-151 (2009).
- 21 Ou, J. Y., Plum, E., Zhang, J. F. & Zheludev, N. I. An electromechanically reconfigurable plasmonic metamaterial operating in the near-infrared. *Nature Nanotechnology* **8**, 252-255, doi:DOI 10.1038/nnano.2013.25 (2013).
- 22 Tao, H. *et al.* MEMS Based Structurally Tunable Metamaterials at Terahertz Frequencies. *J Infrared Millim Te* **32**, 580-595, doi:DOI 10.1007/s10762-010-9646-8 (2011).
- 23 Tao, H. *et al.* Reconfigurable Terahertz Metamaterials. *Physical Review Letters* **103**, doi:Artn 147401
Doi 10.1103/Physrevlett.103.147401 (2009).
- 24 Ma, F. S., Lin, Y. S., Zhang, X. H. & Lee, C. Tunable multiband terahertz metamaterials using a reconfigurable electric split-ring resonator array. *Light-Sci Appl* **3**, doi:ARTN e171
DOI 10.1038/lsa.2014.52 (2014).
- 25 Pryce, I. M., Aydin, K., Kelaita, Y. A., Briggs, R. M. & Atwater, H. A. Highly Strained Compliant Optical Metamaterials with Large Frequency Tunability. *Nano Letters* **10**, 4222-4227, doi:Doi 10.1021/Nl102684x (2010).
- 26 Sensale-Rodriguez, B. *et al.* Broadband graphene terahertz modulators enabled by intraband transitions. *Nature communications* **3** (2012).
- 27 Sensale-Rodriguez, B. *et al.* Unique prospects for graphene-based terahertz modulators. *Applied Physics Letters* **99** (2011).
- 28 Ju, L. *et al.* Graphene plasmonics for tunable terahertz metamaterials. *Nature Nanotechnology* **6**, 630-634 (2011).
- 29 Sensale-Rodriguez, B., Yan, R. S., Liu, L., Jena, D. & Xing, H. G. Graphene for Reconfigurable Terahertz Optoelectronics. *P IEEE* **101**, 1705-1716 (2013).
- 30 Tassin, P., Koschny, T. & Soukoulis, C. M. Graphene for Terahertz Applications. *Science* **341**, 620-621 (2013).
- 31 Mak, K. F., Ju, L., Wang, F. & Heinz, T. F. Optical spectroscopy of graphene: From the far infrared to the ultraviolet. *Solid State Commun* **152**, 1341-1349, doi:DOI 10.1016/j.ssc.2012.04.064 (2012).
- 32 Rouhi, N. *et al.* Terahertz graphene optics. *Nano Res* **5**, 667-678, doi:DOI 10.1007/s12274-012-0251-0 (2012).
- 33 Liu, P. Q. *et al.* Highly tunable hybrid metamaterials employing split-ring resonators strongly coupled to graphene surface plasmons. *Nature communications* **6**, 8969, doi:10.1038/ncomms9969 (2015).
- 34 Lee, S. H. *et al.* Switching terahertz waves with gate-controlled active graphene metamaterials. *Nature Materials* **11**, 936-941, doi:Doi 10.1038/Nmat3433 (2012).
- 35 Emani, N. K. *et al.* Electrically Tunable Damping of Plasmonic Resonances with Graphene. *Nano Letters* **12**, 5202-5206, doi:Doi 10.1021/Nl302322t (2012).
- 36 Yao, Y. *et al.* Broad Electrical Tuning of Graphene-Loaded Plasmonic Antennas. *Nano Letters* **13**, 1257-1264, doi:Doi 10.1021/Nl3047943 (2013).
- 37 Kim, J. *et al.* Electrical Control of Optical Plasmon Resonance with Graphene. *Nano Letters* **12**, 5598-5602, doi:Doi 10.1021/Nl302656d (2012).

- 38 Lee, S. H., Choi, J., Kim, H. D., Choi, H. & Min, B. Ultrafast refractive index control of a terahertz graphene metamaterial. *Sci Rep-Uk* **3**, doi:Artn 2135
Doi 10.1038/Srep02135 (2013).
- 39 Polat, E. O. & Kocabas, C. Broadband Optical Modulators Based on Graphene Supercapacitors. *Nano Letters* **13**, 5851-5857 (2013).
- 40 Baylam, I. *et al.* Femtosecond pulse generation with voltage-controlled graphene saturable absorber. *Opt Lett* **39**, 5180-5183 (2014).
- 41 Polat, E. O., Balci, O. & Kocabas, C. Graphene based flexible electrochromic devices. *Sci Rep-Uk* **4** (2014).
- 42 Balci, O., Polat, E. O., Kakenov, N. & Kocabas, C. Graphene-enabled electrically switchable radar-absorbing surfaces. *Nature communications* **6**, doi:Artn 6628
10.1038/Ncomms7628 (2015).
- 43 Xia, J. L., Chen, F., Li, J. H. & Tao, N. J. Measurement of the quantum capacitance of graphene. *Nature Nanotechnology* **4**, 505-509, doi:Doi 10.1038/Nnano.2009.177 (2009).
- 44 Bae, S. *et al.* Roll-to-roll production of 30-inch graphene films for transparent electrodes. *Nature Nanotechnology* **5**, 574-578 (2010).
- 45 Jackson, J. D. *Classical electrodynamics*. . Vol. 3 (Wiley, 1962).
- 46 Lee, J. *et al.* Switching Individual Quantum Dot Emission through Electrically Controlling Resonant Energy Transfer to Graphene. *Nano Letters* **14**, 7115-7119, doi:Doi 10.1021/Nl503587z (2014).
- 47 Koppens, F. H. L., Chang, D. E. & de Abajo, F. J. G. Graphene Plasmonics: A Platform for Strong Light-Matter Interactions. *Nano Letters* **11**, 3370-3377 (2011).
- 48 Sun, S. L. *et al.* Gradient-index meta-surfaces as a bridge linking propagating waves and surface waves. *Nature Materials* **11**, 426-431, doi:10.1038/NMAT3292 (2012).
- 49 Chen, H. Y., Chan, C. T. & Sheng, P. Transformation optics and metamaterials. *Nature Materials* **9**, 387-396, doi:10.1038/nmat2743 (2010).
- 50 Cui, T. J., Qi, M. Q., Wan, X., Zhao, J. & Cheng, Q. Coding metamaterials, digital metamaterials and programmable metamaterials. *Light-Sci Appl* **3**, doi:ARTN e218
10.1038/lsa.2014.99 (2014).
- 51 Della Giovampaola, C. & Engheta, N. Digital metamaterials. *Nature Materials* **13**, 1115-1121, doi:10.1038/NMAT4082 (2014).

Acknowledgments: This work was supported by the Scientific and Technological Research Council of Turkey (TUBITAK) grant no.: 114F052. O.B. and N.K. acknowledge the fellowship provided by TUBITAK-BIDEB 2211 and 2215.